IPPI
Polyolefins Journal, Vol. 12, No. 2 (2025)
DOI: 10.22063/POJ.2025.35626.1344
ORIGINAL PAPER

Computational fluid dynamics study of polyethylene/ ethylene vinyl acetate blend morphology development in a spinneret by volume of fluid method

Parisa Mohammadzadeh Pakdel[1,3], Reza Yegani[1,3], Mahdi Salami Hosseini[2,3], Elham Shokri[4*]

[1]Faculty of Chemical Engineering, Sahand University of Technology, Sahand New Town, Post box: 51335/1996, Tabriz, Iran
[2]Faculty of Polymer Engineering, Sahand University of Technology, Sahand New Town, Post box: 51335/1996, Tabriz, Iran
[3]Membrane Technology Research Center, Sahand University of Technology, Sahand New Town, Post box: 51335/1996y, Tabriz, Iran
[4]Department of Chemical Engineering, University of Bonab, Bonab, Iran

Received: 28 December 2024, Accepted: 1 March 2025

ABSTRACT

In the current study, the flow field and morphology development of a polyethylene (PE) and ethylene vinyl acetate (EVA) blend were investigated numerically during extrusion through a spinneret using Fluent 6.3.26 software. The interface of the two phases was tracked using the volume of fluid (VOF) method. In a conventional spinneret, EVA droplets near the walls break up due to the high shear rate, while the central droplet deforms without breaking up. To enhance the breakup of EVA droplets, the effects of device geometry, including the spinneret angle and the presence of one or two lamps, were investigated in detail. The numerical results indicated that a decrease in the spinneret angle from 60° to 45° causes the central droplet to become more elongated in the flow direction. Additionally, the results showed that the presence of one or two lamps in the conical zone of the spinneret causes a portion of the central droplet to break up. **Polyolefins J (2025) 12: 73-84**

Keywords: Spinneret; morphology; computational fluid dynamics; flow field; VOF method.

INTRODUCTION

Polymer blends have rapidly attracted worldwide attention and become a new field of membrane research because they provide a simple way of obtaining desirable properties without synthesizing new polymers [1,2]. The advantage of using polymer blends is the improvement of hydrophilicity in membranes, which reduces fouling [3]. Ethylene vinyl acetate (EVA), a hydrophilic polymer, is thermodynamically compatible with hydrophobic polyethylene (PE). However, these two polymers are immiscible due to their positive enthalpy of mixing and high molecular weight, which results in a minimal contribution of entropy of mixing [4,5]. The immiscible blend morphology consists of a droplet-matrix structure, where the size scale and distribution of dispersed phase droplets across the hollow fiber membrane cross-section depend on the flow conditions in the spinneret. It has been shown that the distribution of immiscible droplets significantly impacts the final properties and microscopic structure of blend hollow fiber membranes. A more uniform droplet

*Corresponding Author - E-mail: Elh.shokri@ubonab.ac.ir

distribution leads to better structural and operational properties [6]. It is anticipated that the development of an appropriate morphology in hollow fibers is strongly influenced by the flow field inside the spinneret [7].

Generally, two opposing processes—droplet breakup and coalescence—determine the final mean size of dispersed droplets. Many researchers have studied droplet deformation and breakup in elongation and shear flow fields. Taylor [8] was the first to introduce two dimensionless parameters that control droplet deformation behavior for an isolated Newtonian droplet in a steady, simple shearing flow of a surrounding immiscible Newtonian fluid in the small-deformation limits. These two controlling parameters are the viscosity ratio between the droplet and matrix phases (P) and the Capillary number (Ca) [9]. Grace's experimental results showed that droplet breakup is easier in an elongational flow field than in a simple shear field [10]. They also showed that when the viscosity ratio in the shear flow field is higher than four, the critical capillary number becomes infinite, implying that no droplet breakup will occur.

As a result, understanding the flow field and droplet deformation are crucial for designing an appropriate spinneret for blend hollow fiber membranes.

The effect of spinneret geometry on the one-phase flow field and fiber properties has been investigated by several researchers. Shilton [11] determined the velocity, shear rate, and shear stress profiles induced within the concentric annulus spinneret for a power-law dope solution. Chung *et al.* [12] studied the effect of dope shear rate within a straight annular spinneret during hollow fiber spinning on the properties of PES ultrafiltration (UF) hollow fiber membranes. Experimental results indicated that an increase in shear rate leads to the formation of a dense skin layer due to greater molecular orientation, which results in compacted polymer chains. They identified a critical shear rate value for lower polymer concentrations, which improves performance in separation processes. Qin *et al.* [13] investigated the effect of shear stress within the spinneret on the properties of PES hollow fiber UF membranes. Their results suggested that for higher polymer concentrations, the shear rate had no significant impact on membrane performance. However, for lower polymer concentrations, the shear rate's effect on membrane performance is crucial. Cao *et al.* [14] investigated the effect of elongation and shear rates in spinnerets on the gas separation performance of PES hollow fiber membranes. They used three types of spinnerets with flow angles of 60°, 75°, and 90°. Their combined simulation and experimental results showed that elongation rate impacts permselectivity more than permeance, while shear rate impacts permeance more than permselectivity. Karuppasamy *et al.* [15] simulated the flow behavior of different power-law fluids in spinnerets with varying flow angles of 90°, 75°, 60°, and 30°, and at different flow rates. Their simulation results showed that the shear rate is higher on the inner and outer surfaces of the spinneret, and it increases as the flow angle decreases. They also suggested that the dope flow rate should be selected based on the rheological properties of the dope solution, such as the power-law index and consistency factor, to avoid the formation of finger-like macrovoids in the hollow fiber membrane.

Computational fluid dynamics (CFD) is a versatile method that provides valuable information on flow field details. The interface between two immiscible phases can be tracked using various CFD techniques, such as the volume tracking method, the level set method (LSM), front tracking method, lattice Boltzmann method (LBM), and fractional volume of fluid (VOF) method [16-18].

In the current study, the VOF method based on the commercial code, Fluent 6.3.26 software, was used to track the interface of PE and EVA phases during extrusion through the various designed spinnerets. To the best of our knowledge, there has been no report on the morphology development of blend dope solution in the spinneret. To understand EVA droplets breakup, the flow field in various designed spinnerets was also simulated.

NUMERICAL SIMULATION

Mathematical formulations

The assumptions of two-dimensional, incompressible, isothermal, and laminar flow were made to model two fluid phases consisting of three non-Newtonian droplets of EVA, each with a radius of 200 μm, suspended in a continuous non-Newtonian PE fluid phase. Due to the symmetrical geometry of the spinneret, only half of it was simulated using Cartesian coordinates. The pathway of the blend dope solution was meshed using GAMBIT software version 2.2.30. A commercial computational fluid dynamics software package, Fluent 6.3.26, based on a finite volume approach, was used to solve the continuity and Navier-Stokes equations (Eqs. 1 and 2), coupled with the empirical

viscosity equation for the two phases (Eq. 7). Physical properties, such as density and viscosity, at any point in the domain were determined from the volume-fraction-weighted average properties of the two fluids.

$$\frac{\partial \rho}{\partial t} + \nabla.(\rho \vec{u}) = 0 \quad (1)$$

$$\frac{\partial (\rho \vec{u})}{\partial t} + \nabla.(\rho \vec{u}\vec{u}) = -\nabla \overline{\overline{P}} - \nabla.\overline{\overline{\tau}} + \vec{F} \quad (2)$$

where, $\vec{u}$ denotes the velocity vector, $\overline{\overline{P}}$ and $\overline{\overline{\tau}}$ the pressure and stress tensors, and ρ the density of fluid. Additionally, $\vec{F}$ is a source term including gravitational force and the interfacial tension force ($\vec{F}_s$) introduced as a body force acting on grid cells that contain the interface. The value of $\vec{F}_s$ is given by the following equation.

$$\vec{F}_s = \sigma k \vec{n} \quad (3)$$

$$k = -\nabla.(\frac{\nabla \alpha}{|\nabla \alpha|}) \quad (4)$$

where, σ denotes the surface tension coefficient, $\vec{n}$ is the unite vector normal to the interface, α is the VOF volume fraction tracking the interface of dispersed and continuous phases, and k is the curvature of the interface which is defined by Eq. 4 [19].

The rheological constitutive equation that relates the stress tensor ($\overline{\overline{\tau}}$) to the rate-of-strain tensor is the generalized Newtonian model [20].

$$\overline{\overline{\tau}} = 2\eta.\overline{\overline{\Delta}} = 2\eta(\frac{\nabla \vec{u} + (\nabla \vec{u})^T}{2}) \quad (5)$$

Where $\nabla \vec{u}$, $(\nabla \vec{u})^T$, and $\overline{\overline{\Delta}}$ are velocity gradient, transpose of velocity gradient, and rate-of-strain tensor, respectively. Rate-of-strain tensor is defined in two-dimensional Cartesian coordinates as follows.

$$\overline{\overline{\Delta}} = \frac{1}{2}\begin{pmatrix} 2\frac{\partial u_x}{\partial x} & \frac{\partial u_x}{\partial y} + \frac{\partial u_y}{\partial x} \\ \frac{\partial u_y}{\partial x} + \frac{\partial u_x}{\partial y} & 2\frac{\partial u_y}{\partial y} \end{pmatrix} \quad (6)$$

According to Cross Law, the viscosity (η) and the magnitude of the rate-of-strain tensor ($\dot{\gamma}$) are expressed as Eqs. 7 and 8, respectively. The parameters of the cross model including viscosity at zero strain rate (η_0) and relaxation time (λ(s)) for PE and EVA are tabulated in Table. 1. Also, the surface tension coefficient between two phases was adjusted to 0.001N/m.

$$\eta = \frac{\eta_0}{1 + (\lambda \dot{\gamma})^{1-m}} \quad (7)$$

$$\dot{\gamma} = \left[2((\frac{\partial u_x}{\partial x_x})^2 + (\frac{\partial u_y}{\partial x_y})^2) + (\frac{\partial u_x}{\partial x_y} + \frac{\partial u_y}{\partial x_x})^2 \right]^{\frac{1}{2}} \quad (8)$$

The volume of fluid (VOF) method was used to track the interface between the droplet and matrix phases. The volume fraction of each phase in each computational cell α_i is computed by solving a passive transport equation as given by the following equation:

$$\frac{\partial}{\partial t}(\alpha_d \rho_d) + \nabla.(\alpha_d \rho_d \vec{u}) = 0 \quad (9)$$

$$\alpha_d + \alpha_m = 1 \quad (10)$$

Boundary conditions

To solve the governing equations, boundary conditions were applied for spinnerets including, velocity inlet boundary condition at the inlet, outflow boundary condition at the outlet, and no-slip boundary condition at the spinneret walls. The simulation captured interface of two phases under the unsteady state condition. In all cases, the axial inlet velocity was considered 0.0013 m/s.

Details on the domain and mesh

The geometry and dimensions of spinnerets were depicted in Figures 1a-1d including: a) conventional spinneret, b) spinneret with a conical angle of 45°, c) spinneret with a lamp depth of 0.18 mm, and d) spinneret with two lamps depth of 0.18 mm and 0.6 mm in conical section. To better describe the flow field and morphology development in the spinnerets, three sections were considered in each design including section-a, section-b, and section-c. The quadratic structured mesh with an interval size of 0.01 for all designed spinnerets was generated using Gambit 2.2.30 software.

Table 1. Density and cross model parameters of PE and EVA [11].

Material	ρ (kg/m³)	η_0(Pa.s)	λ(s)	m
PE	895	6015	0.26	0.45
EVA	923	5980	1.2	0.41

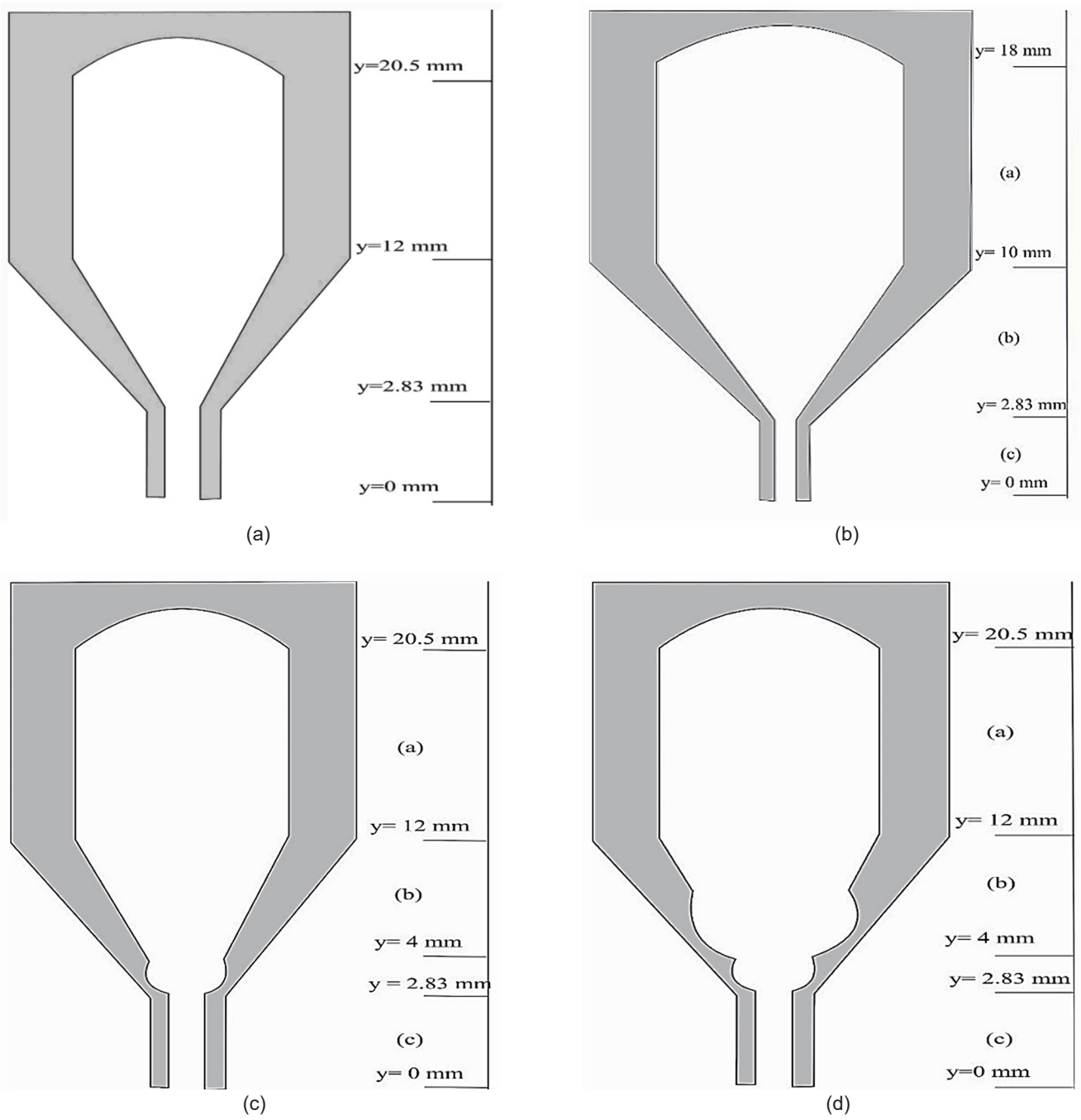

Figure 1. Geometry and dimensions of (a) conventional spinneret, (b) spinneret with a conical angle of 45°, (C) spinneret with a lamp, and (d) spinneret with two lamps in the conical section.

Solution methodology

The governing equations were solved using commercial Fluent 6.3.26 software which uses the finite volume method. To track the interface of two immiscible phases, VOF algorithms were solved using an explicit scheme. The gradients were computed by Green-Gauss cell-based method and the pressure-velocity coupling was performed using the coupled scheme. The body force weighted and QUICK schemes were applied to interpolation of pressure and discretization of momentum equation, respectively. The volume fraction equation was solved using the Geometric reconstruction method. The iteration time step size and maximum iteration per time step were considered 0.001 s and 20, respectively. The iteration stops when the convergence criterion is provided. The convergence criterion for all equations was set to be 1E-6. To prevent the diffusive problem, the global courant number is less than 0.25 [21].

Table 2. Mesh independency analysis for designed spinnerets based on deformation parameter (Def) of the central droplet at y= 16 and 7.8 mm.

Type of Spinneret	Element size	Number of elements	Def at Y= 16 mm	Def at Y= 7.8 mm
Conventional spinneret	0.05	26280	0.15	0.496
Conventional spinneret	0.025	105000	0.18	0.53
Conventional spinneret	0.01	656100	0.22	0.66
Conventional spinneret	0.0075	1166400	0.235	0.682
Spinneret with flow angle of 45°	0.05	24240	0.15	0.65
Spinneret with flow angle of 45°	0.025	96840	0.18	0.68
Spinneret with flow angle of 45°	0.01	605700	0.22	0.73
Spinneret with flow angle of 45°	0.0075	1076400	0.235	0.738
Spinneret with one lamp	0.05	26520	0.15	0.51
Spinneret with one lamp	0.025	106080	0.18	0.543
Spinneret with one lamp	0.01	663000	0.22	0.69
Spinneret with one lamp	0.0075	1178400	0.235	0.712
Spinneret with two lamps	0.05	17219	0.15	0.53
Spinneret with two lamps	0.025	69327	0.18	0.567
Spinneret with two lamps	0.01	601420	0.22	0.734
Spinneret with two lamps	0.0075	1069158	0.235	0.742

Definitions

The mean shear and elongation rates in 2D Cartesian coordinates are calculated using the following equations.

$$\text{Mean Shear Rate} = \sqrt{(\frac{\partial u}{\partial y})^2 + (\frac{\partial v}{\partial x})^2} \quad (11)$$

$$\text{Mean Elongation Rate} = \sqrt{(\frac{\partial u}{\partial x})^2 + (\frac{\partial v}{\partial y})^2} \quad (12)$$

Viscosity ratio (P) is defined as the ratio of viscosities of dispersed to matrix phases and is represented by Eq. 13.

$$P = \frac{\eta_d}{\eta_m} \quad (13)$$

For the numerical investigation of central droplet shape change, the deformation parameter (Def) was used. This parameter was introduced by Taylor and given by the Eq. 14.

$$Def = \frac{L - B}{L + B} \quad (14)$$

where, L and B denote long and short semi-axes of the droplet cross section. For a spherical droplet deformation parameter is zero and for an infinitely extended droplet is one. The capillary number represents the ratio of viscous to interfacial forces which is defined as follows.

$$Ca = \frac{\eta_m \times \dot{\gamma} \times R}{\sigma} \quad (15)$$

where, η_m, R, and σ are the viscosity of the matrix phase, the radius of the droplet, and interfacial tension between matrix and dispersed phases.

Mesh sensitivity analysis

A grid sensitivity analysis is required to assess the dependency of the results of the simulation on element size. To probe mesh independency of simulation, four different element sizes were considered as represented in Table 2. For each element size, the deformation parameter of the central droplet in y= 16 and 7.8 mm of all designed spinnerets was calculated and represented in Table. 2. The results of element sizes of 0.0075 and 0.01 were similar so the element size of 0.01 was selected to mesh all designs of spinnerets. Also, there are enough nodes along the axes to capture the interface of two phases in these mesh sizes. When the element size was selected at 0.005, the time for simulation increased which is a negative point in simulation works.

RESULTS AND DISCUSSION

Flow field development in the conventional spinneret investigating flow behavior is crucial for understanding the mechanism of EVA droplets' deformation and breakup within the spinneret. To this end, the mean

shear rate and mean elongation rate were plotted for different sections of the spinneret. As shown in Figure 2a, the mean shear rate at the center of section-a of the spinneret is zero, with the highest value occurring near the walls. The mean elongation rate is nearly zero in most of section-a, except near the entrance and exit, which is attributed to entrance and exit effects (see Figure 2b). The mean shear and elongation rates for section-b of the spinneret are shown in Figures 2c and 2d, respectively. Both the mean shear and elongation rates increase in the center and near the walls, which is related to the reduction in the cross-section of section-b along the flow direction, affecting flow velocity and the direction of flow. The variations in mean shear and elongation rates in section-c are like those in section-a, so the variation of mean elongation rates in section-c can be neglected. As shown in Figure 2e, the mean shear rate near the walls of the spinneret is higher in section-b than in section-a, which is attributed to the higher flow velocity in this section.

Morphology development of PE and EVA polymer blend in the conventional spinneret

Figures 3a-3h illustrate the development of PE/EVA morphology during flow in section-a of the spinneret. As shown in Figures 3a-3d, the central droplet moves downward without breaking up and elongates moderately along the flow direction. Droplets near the walls elongate more and deform into threads due to the high shear rate (see Figures 3e-3h). The simulation results show that as the droplets transform into threads, their heads become thick and rounded, while the tails of the threads become thin and sharp. Due to the high shear rate applied to the tails of the threads, breakup and the formation of small droplets begin at the thread's tail. The breakup of the threads is attributed to increasing interfacial stresses resulting from the growing interface between the two phases. As seen in Figures 3a-3h, droplets near the walls migrate laterally from their initial positions until they reach a stable equilibrium. This equilibrium position depends on factors such as inlet velocity, surface tension between the two polymers, initial droplet size, and position. This lateral migration positively affects droplet breakup, facilitating easier breakup in this simple shear flow field. Figure 4a shows the variation of the deformation parameter with position. The deformation parameter of the central droplet increases from 0 to 0.22 as the droplet moves from y = 20.5 mm to 19 mm, and then becomes constant as the droplet moves from y = 19 mm to 14.89 mm. The deformation of the central droplet can be attributed to the entrance effect of the flow.

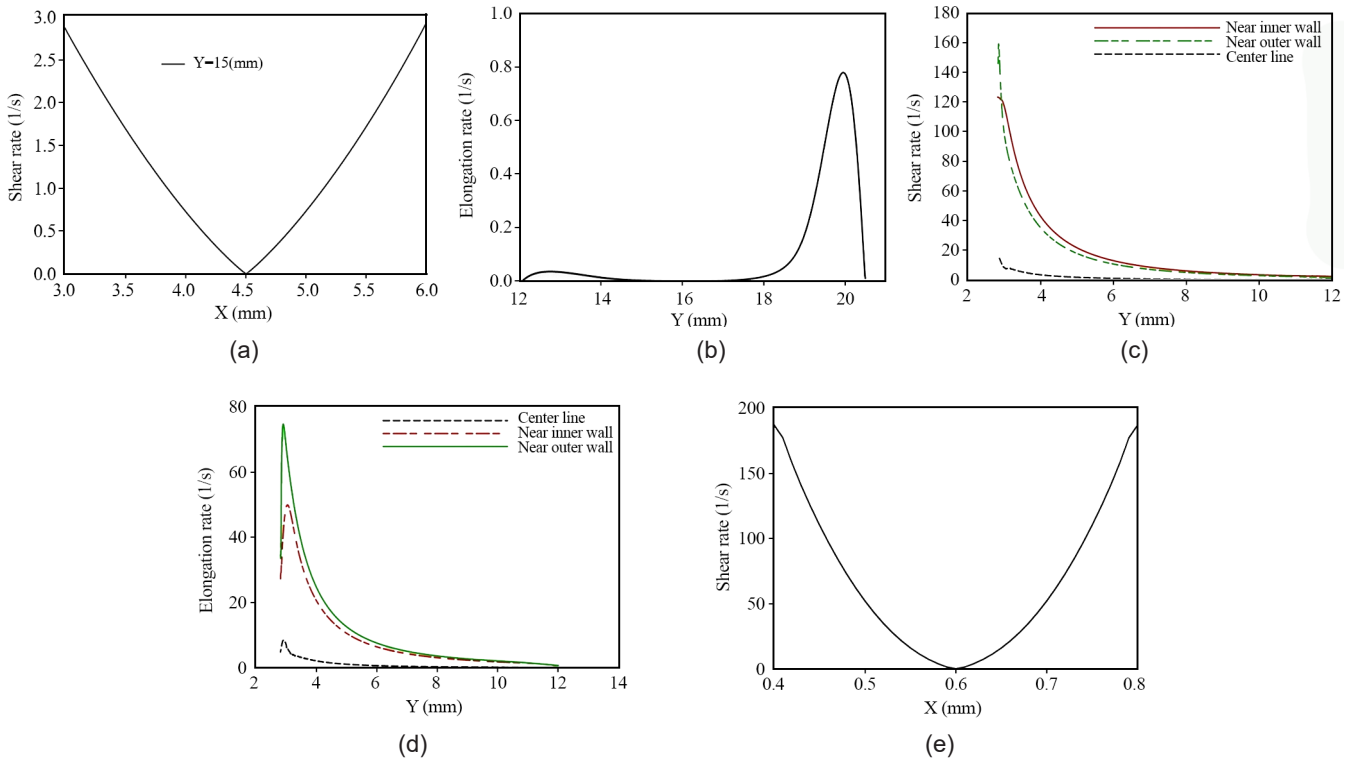

Figure 2. (a) Mean shear rate in cross section of a-section, (b) elongation rate across the central line of a-section, (c) shear rate, (d) elongation rate in b-section, and (e) mean shear rate in cross section of c-section.

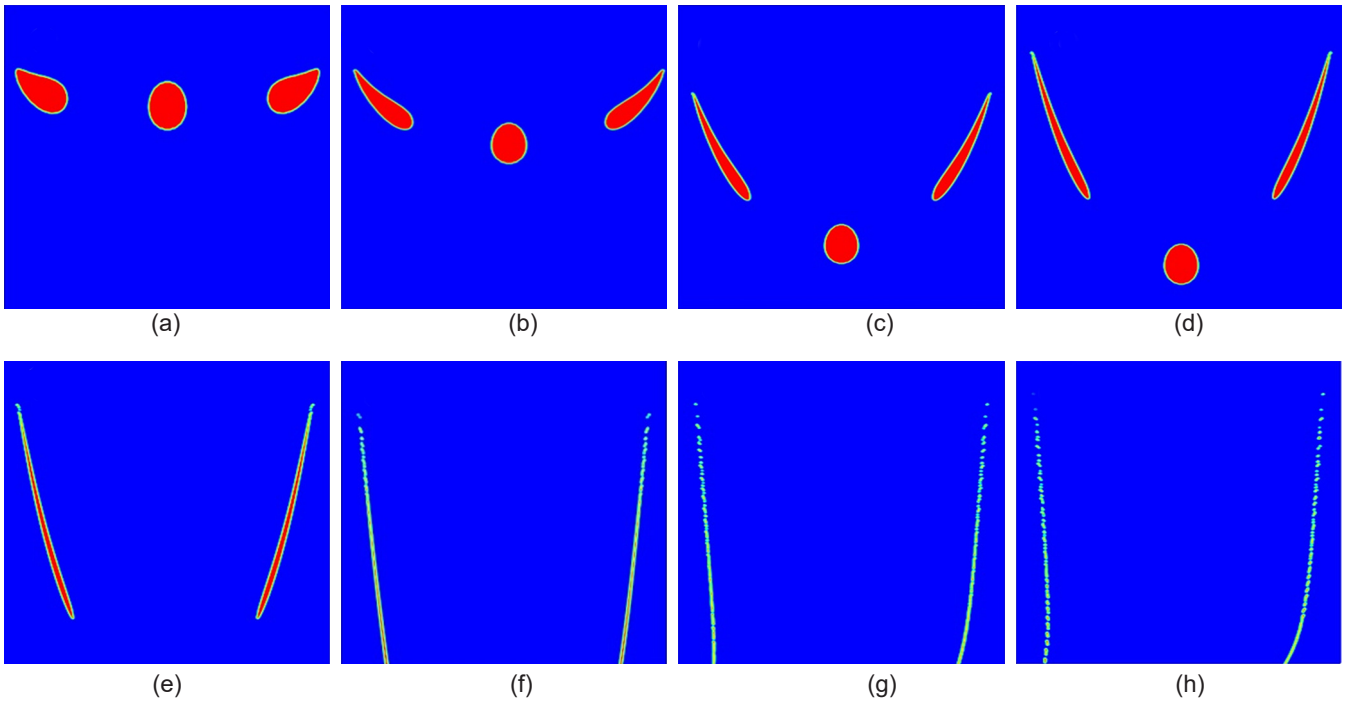

Figure 3. Morphology development of PE/EVA blend in the a-section of spinneret: (a) t=0.25 s, (b) t=0.75 s, (c) t=1.5 s, (d) t=2 s, (e) t= 3.15 s, (f) t= 5.25 s, (g) t=7.5 s, and (h) t=9.15 s.

Theoretically, the possibility of droplet break-up is determined by capillary number and viscosity ratio [22]. As the central droplet moves downstream of the spinneret, the viscosity ratio decreases.

In Figure 4b, the central droplet capillary number has been plotted versus viscosity ratio. It can be seen that the capillary number increases with reducing the viscosity ratio. When capillary number is bigger than one, viscous forces dominate on interfacial forces so interfacial forces do not play a significant role and break up of central droplet is impossible in this section.

Figures 5a and 5b show the changes in the central droplet's shape in section-b of the spinneret. When the central droplet reaches section-b, it elongates along the flow direction and eventually deforms into a thread with rounded ends. This can be attributed to the increased elongation rate caused by the change in flow direction and the reduction in cross-sectional area. The morphology development of droplets near the walls is shown in Figures 5c and 5d. As mentioned earlier, droplets near the walls change shape from spherical to thread-like, and some of them break into small

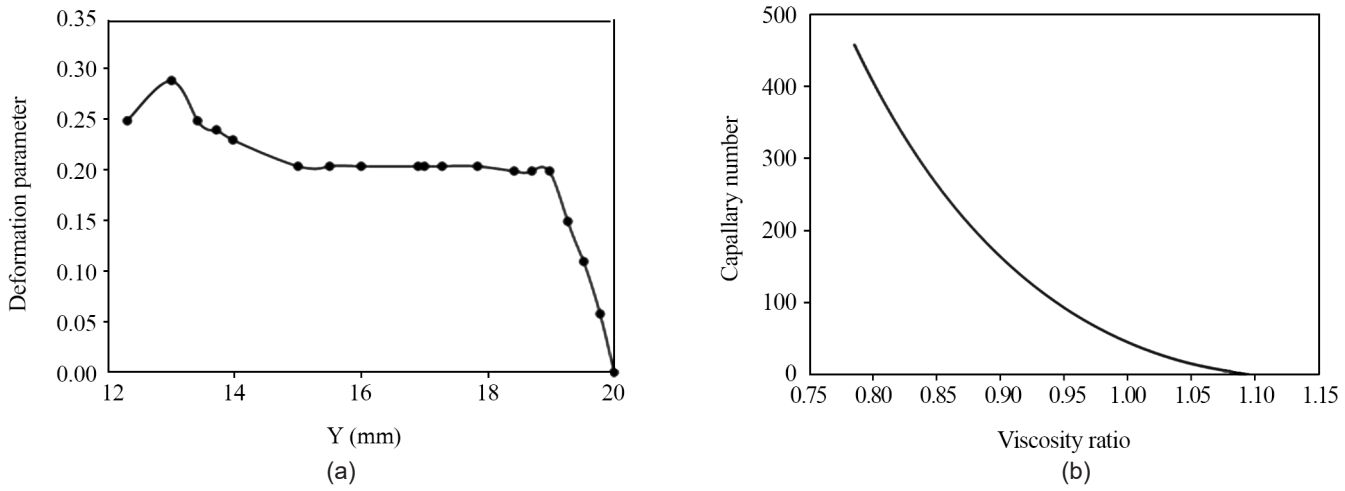

Figure 4. (a) Deformation parameter vs. length, and (b) capillary number vs. viscosity ratio of central droplet in section-a of the spinneret.

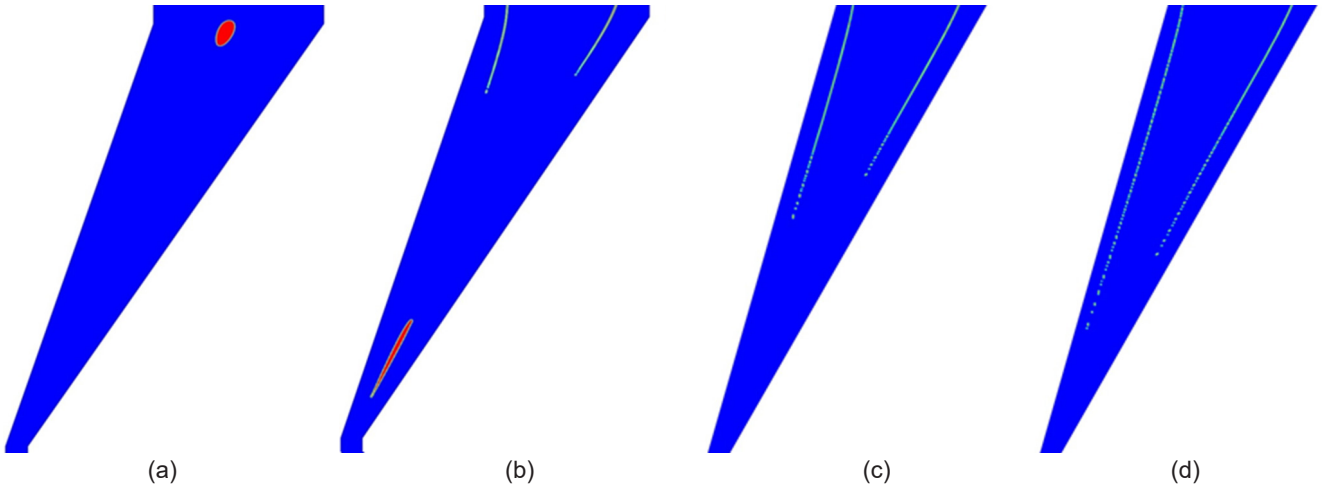

Figure 5. Central droplet deformation (a) t=4.35 s, and (b) t=6.75 s, near walls droplets deformation (c) t=8.55 s, and (d) t=8.7 s along flow direction in section-b of spinneret.

droplets from their tail in section-a. In section-b, these threads break completely from their heads into small droplets, which is related to the increased elongation and shear rates along the flow direction (see Figures 2c and 2d).

Figure 6a shows the central droplet deformation parameter in section-b of the spinneret. The deformation parameter increases along the flow direction, causing the droplet to become more elongated in this section, which is primarily due to the increase in elongation and shear rates. As mentioned earlier, the viscosity ratio decreases along the flow direction. Therefore, as shown in Figure 6b, it can be concluded that the maximum viscous forces are applied to the dispersed phase at the end of section-b. However, the viscous and interfacial forces are not sufficient to break up the central droplet in this section.

Morphology development of central and near walls droplets in section-c is depicted in Figures 7a and 7b. As depicted in Figure 7a, the central thread doesn't break in this section and forms a barrier layer in the cross section of produced blend hollow fiber membranes which reduces filtration performance and mechanical properties of them. Figure 7b demonstrates that produced small droplets don't break in this section, too.

The effect of spinneret geometry on the flow field and morphology development of PE/EVA blend

As mentioned earlier, the size of EVA droplets is strongly dependent on the flow field, so their size can be controlled by variations in the flow field. In this section of the current study, the geometry of the conventional spinneret is modified to improve the morphology of

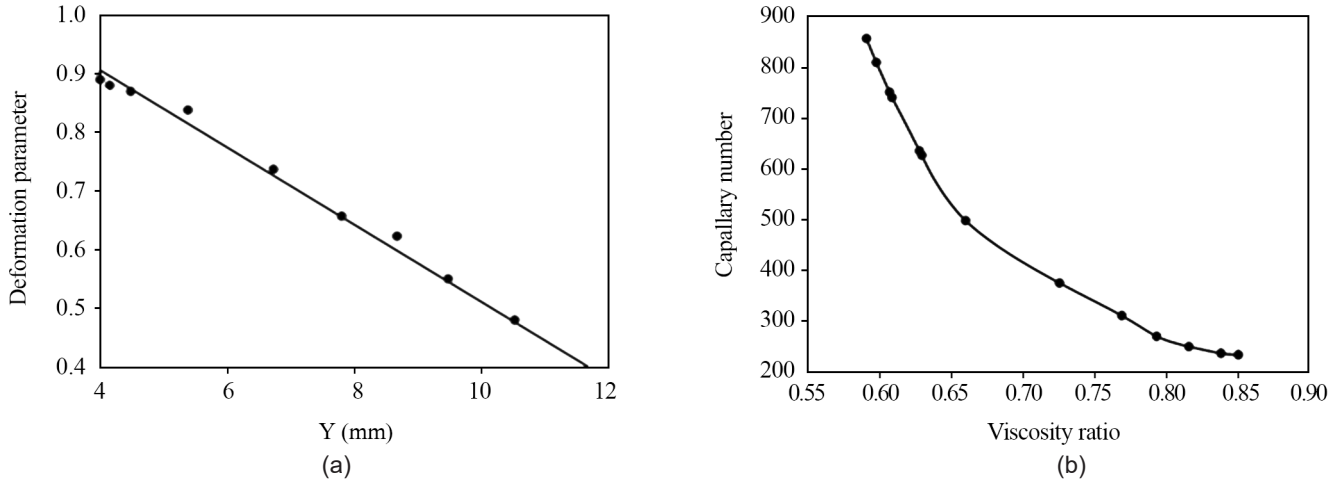

Figure 6. (a) Deformation parameter vs. length, and (b) capillary number vs. viscosity ratio of central droplet in section-b of the spinneret.

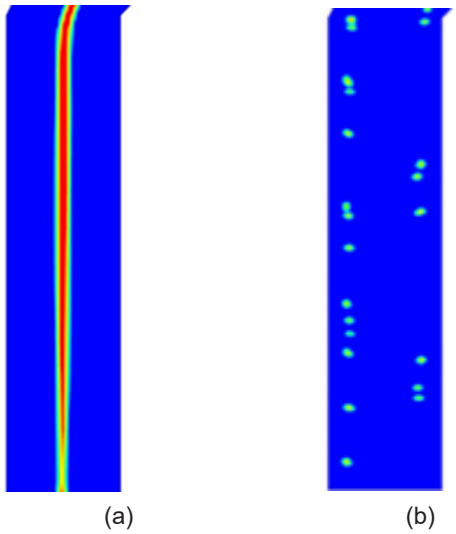

Figure 7. Morphology development of (a) central droplet, and (b) near walls droplets in the section-c of the spinneret.

PE/EVA blend hollow fiber membranes. Based on the results from the previous section, maximum forces are applied to the dispersed phase in section-b of the spinneret, so geometric modifications must be applied in this section. The effects of flow angle, the presence of one or two lamps in the conical section on mean shear and elongation rates, and EVA droplet breakup are discussed in the following sections.

The effect of spinneret geometry on the flow field

Figure 8 demonstrates the effect of flow angle, the presence of one and two lamps in the conical. Figure 8 demonstrates the effect of flow angle, as well as the presence of one or two lamps in the conical section, on mean shear and elongation rates in section-b of the spinneret. To investigate the effect of flow angle on mean shear and elongation rates, the angle was reduced from 60° to 45°. Reducing the conical section angle significantly increases the mean shear and elongation rates due to greater changes in the flow direction (see Figure 8a). The effect of a single lamp on mean shear and elongation rates is shown in Figures 8c and 8d, respectively. In the converging part of the lamp, where the flow's cross-sectional area decreases, both shear and elongation rates increase, reaching their highest values in the throat of the lamp. After the flow passes through the throat, both shear and elongation rates decrease due to the increased cross-sectional area. As the flow approaches the interface between sections b and c, the shear and elongation rates increase again due to the end effects of the flow. The effect of two lamps on mean shear and elongation rates is shown in Figures 8e and 8f, respectively. The first peak corresponds to the first lamp, and the second peak corresponds to the second lamp. Since the depth of the second lamp is greater than that of the first, the

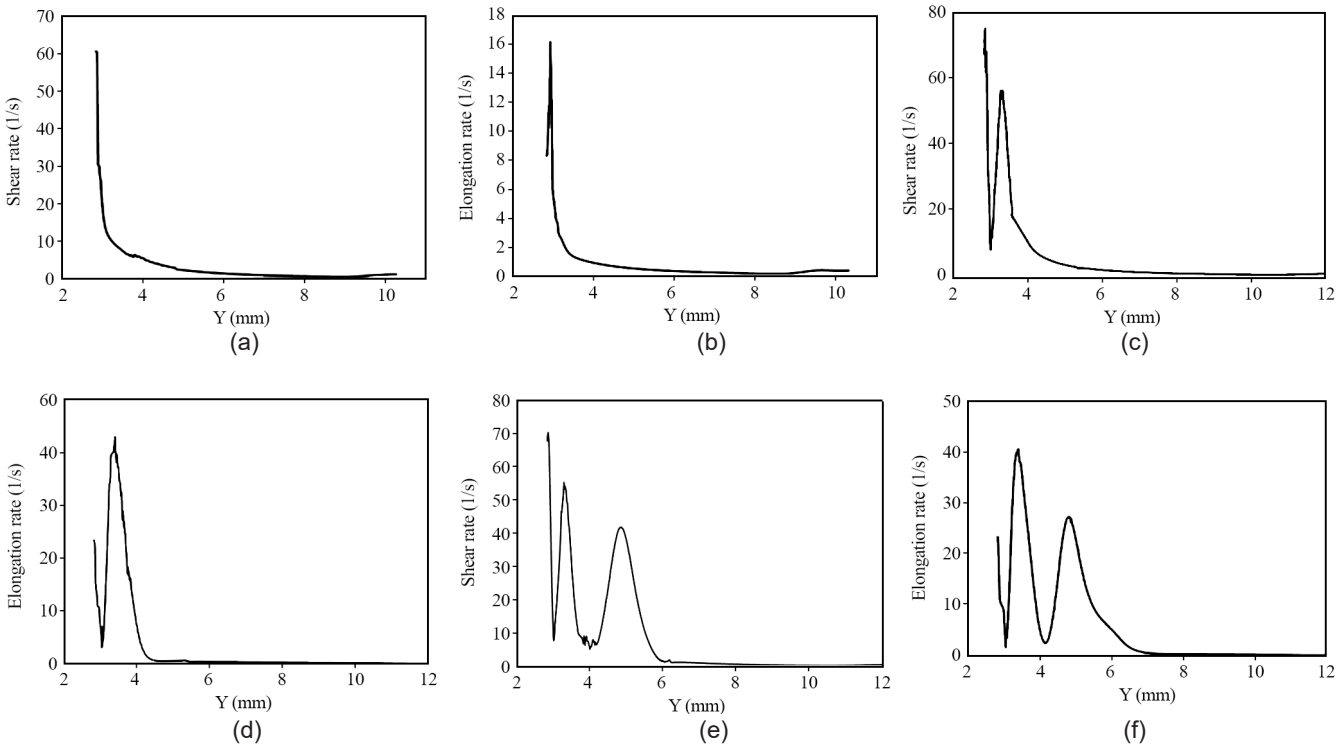

Figure 8. (a) Mean shear rate, (b) mean elongation rate in the flow angle of 45◦, (c) mean shear rate, (d) mean elongation rate in presence of one lamp, and (e) mean shear rate, (f) mean elongation rate in presence of two lamps.

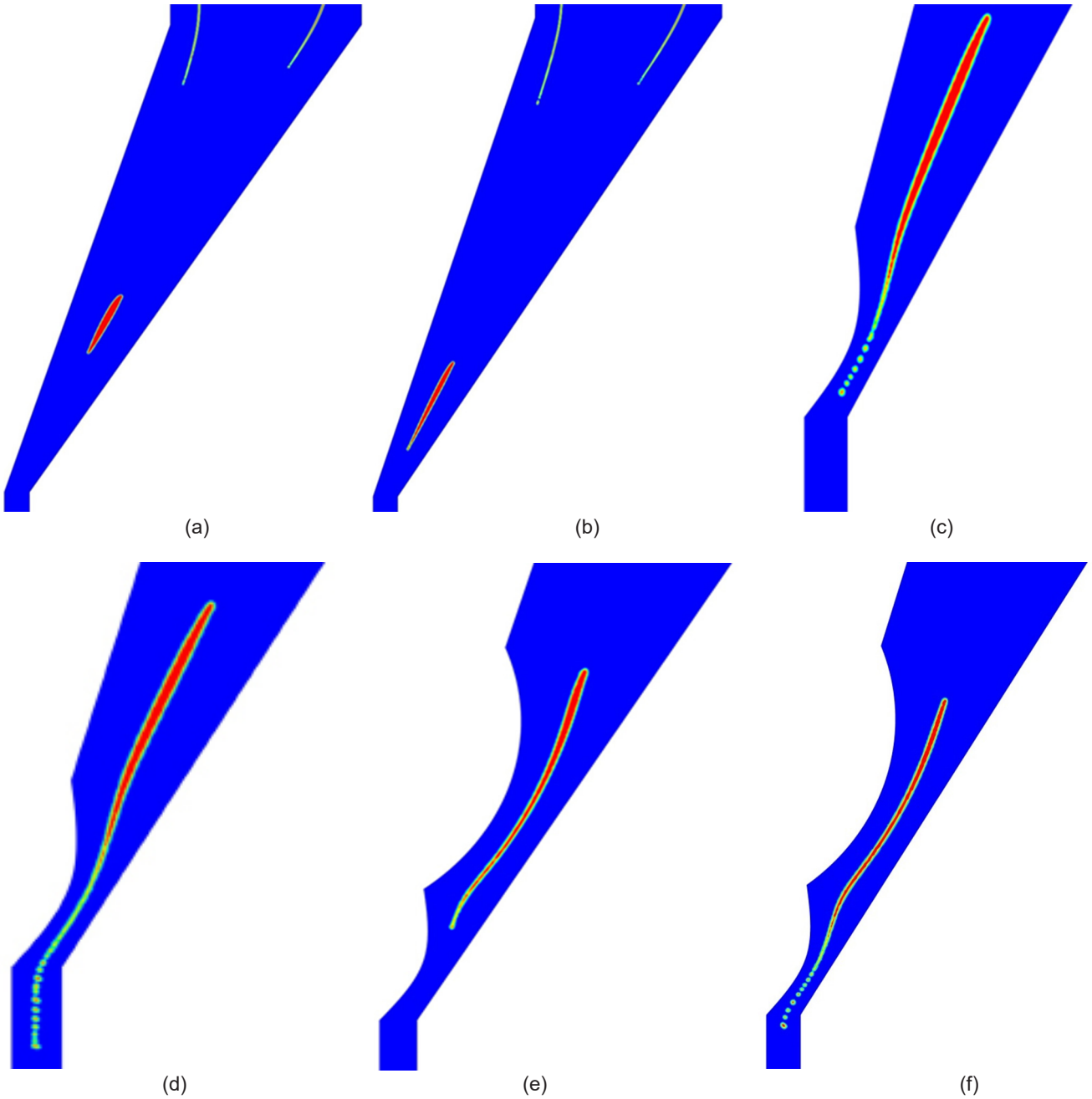

Figure 9. Morphological evolution of the central droplet in the spinneret under different conditions: (a, b) with a flow angle of 45°, (c, d) under illumination from a single lamp, and (e, f) under illumination from two lamps.

mean shear and elongation rates in the second lamp are higher than in the first.

The effect of spinneret geometry on the morphology of PE/EVA

The morphology development of PE/EVA in the conical section of the spinneret with a 45° angle is shown in Figures 9a and 9b. The central droplet elongates more in this spinneret compared to the conventional one, due to higher shear and elongation rates, but it does not break up. Therefore, reducing the spinneret angle has a minimal effect on improving the morphology. The morphology development of PE/EVA in the conical section of the spinneret with one lamp is shown in Figures 9c and 9d. A portion of the central droplet breaks up from the head due to experiencing higher shear and elongation rates compared to the tail, leading to improved properties of the PE/EVA blend hollow fiber membranes. To enhance the breakup of the central droplet in the spinneret, two lamps are introduced in section-b. As depicted in Figures 9e and 9f, part of the central droplet breaks up due to

the high shear and elongation rates in this spinneret design. It is worth noting that the effect of two lamps on morphology enhancement is similar to that of one lamp.

CONCLUSION

In this study, the flow field and morphology development of PE/EVA blend during extrusion in the spinneret were investigated using Fluent 6.3.26 software. To track the interface of two phases, the VOF method was used. Simulation results showed that near walls droplets break up due to the experience of a high shear rate but central droplets don't break up leading to the weak mechanical strength of fabricated membranes. The effect of spinneret angle and the presence of one and two lamps were investigated. Flow field studies showed that higher elongation and shear rates are exerted on droplets in the spinneret with lamps in comparison to the spinneret with the angle of 45°. Variation of spinneret angle had not effect on central droplets break up but the presence of one lamp enhanced central droplets. The effect of the two lamps on the breakup of the central droplets was the same as that of one lamp.

CONFLICTS OF INTEREST

The authors declared that there is no conflict of interest to state.

REFERENCES

1. Utracki LA, Shi ZH (2004) Development of polymer blend morphology during compounding in a twin-screw extruder. Part I: Droplet dispersion and coalescence: A review. Polym Eng Sci 32: 1824-1833
2. Yong WF, Zhang H (2020) Recent advances in polymer blend membranes for gas separation and pervaporation. Prog Mater Sc 116: 100713
3. Kadanyo S, Gumbi NN, Matindi CN, Dlamini DS, Hu Y, Cui Z, Wang H, Hu M, Li J (2022) Enhancing compatibility and hydrophilicity of polysulfone/poly (ethylene-co-vinyl alcohol) copolymer blend ultrafiltration membranes using polyethylene glycol as hydrophilic additive and compatibilizer. Separ Purif Technol 287: 120523
4. Fortelný I, Živný A (2003) Extensional flow induced coalescence in polymer blends. Rheol Acta 42: 454-461
5. Velayutham TS (2024) Miscibility and immiscibility in PVC-based blends, IPNs, and gels. In: Poly(vinyl chloride)-based blends, IPNs, and gels Elsevier, pp: 377-400
6. Xiang S, Tang X, Rajabzadeh S, Zhang P, Cui Z, Matsuyama H (2022) Fabrication of PVDF/EVOH blend hollow fiber membranes with hydrophilic property via thermally induced phase process. Separ Purif Techno 301: 122031
7. Perera HS, Ernst KJ, Tafreshi HV, Khan SA (2024) Viscoelastic fluid stresses in the formation and shaping of melt-spun hollow fibers. ACS Appl Eng Mater 3: 75-84
8. Wilczyński K, Tyszkiewicz A, Szymaniak Z (2002) Modeling for morphology development during single-screw extrusion of LDPE/PS blend. J Mater Process Technol 109: 320-323
9. Tanpaiboonkul P, Lerdwijitjarud W, Sirivat A, Larson RG (2007) Transient and steady-state deformations and breakup of dispersed-phase droplets of immiscible polymer blends in steady shear flow. Polymer 48: 3822-3835
10. Janssen J, Meijer H (2002) Droplet breakup mechanisms: Stepwise equilibrium versus transient dispersion. J Rheol 37: 597-608
11. Shilton SJ (2002) Flow profile induced in spinneret during hollow fiber membrane spinning. J Appl Polym Sci 65: 1359-1362
12. Chung TS, Qin JJ, Gu J (2002) Effect of shear rate within the spinneret on morphology, separation performance and mechanical properties of ultrafiltration polyethersulfone hollow fiber membranes. Chem Eng Sci 55: 1077-1091
13. Qin JJ, Wang R, Chung TS (2002) Investigation of shear stress effect within a spinneret on flux, separation and thermomechanical properties of hollow fiber ultrafiltration membranes. J Membrane Sci 175: 197-213
14. Cao C, Chung TS, Chen SB, Dong ZJ (2004) The study of elongation and shear rates in spinning process and its effect on gas separation performance of Poly(ether sulfone) (PES) hollow fiber membranes. Chem Eng Sci 59: 1053-1062
15. Selvam K, Suresh K, Karunanithi B (2021) Assessment of the flow behavior of power-law fluids in spinnerets. Chem Eng Res Des 176: 134-145
16. Ning H, Qian S, Zhou T (2023) Applications of

level set method in computational fluid dynamics: A review. Intl J Hydromechatronics 6: 1
17. Fakhreddine A (2024) Numerical simulation and modeling of two-phase flows using the volume-of- fluid method, University of Minnesota, Ph.D. dissertation
18. Li B, Zhang H, Fu S, Su W, Wang Y, Wang L (2024) Simulation of single droplet deformation and breakup in shear flow by the phase-field lattice Boltzmann method. Ind Eng Chem Res 63: 22104-22117
19. Deng C, Wang H, Huang W, Cheng S (2017) Numerical and experimental study of oil-in-water (O/W) droplet formation in a co-flowing capillary device. Colloids Surf A: Physicochem Eng Asp 533: 1-81
20. Aloku GO, Yuan XF (2010) Numerical simulation of polymer foaming process in extrusion flow. Cheml Eng Sci 65: 3749-3761
21. Pan D, Zhang Y, Zhang T, Li B (2021) Flow regimes of polymeric fluid droplet formation in a co-flowing microfluidic device. Colloid Interface Sci Commun 42: 100392
22. Zhang T, Shao T, Zhang Y, Pan D, Huang W, Li B (2021) Effect of interface deformation on hydrodynamics of liquid–liquid two-phase flow in a confined microchannel. Chem Eng J 427: 131956